*How to Cite:* Rakisheva, S.R., Nurpeisova, D.T., Zhumabayev, A.M., Parmanbek, N., Barsbay, M. & Mashentseva, A.A. (2025). Galvanic Replacement-Assisted Synthesis of Cu–Ag Composite Membrane Catalysts for Potassium Ferricyanide Reduction. *Eurasian Journal of Chemistry, 30, 3(119), 129-142.* https://doi.org/10.31489/2959-0663/3-25-6

*Article*

Received: 26 May 2025 | Revised: 13 August 2025 |
Accepted: 18 August 2025 | Published online: 26 September 2025

UDC 544.478-03; 544-971

https://doi.org/10.31489/2959-0663/3-25-6

Saniya R. Rakisheva[1, 2], Dinara T. Nurpeisova[1, 2], Alisher M. Zhumabayev[1,2], Nursanat Parmanbek[1], Murat Barsbay[3], Anastassiya A. Mashentseva[1, 2]*

[1]*Institute of Nuclear Physics of the Republic of Kazakhstan, Almaty, Kazakhstan;*
[2]*L.N. Gumilyov Eurasian National University, Astana, Kazakhstan;*
[3]*Department of Chemistry, Polymer Chemistry Division, Hacettepe University, Ankara, Türkiye*
*(*Corresponding author's e-mail: a.mashentseva@inp.kz)*

# Galvanic Replacement-Assisted Synthesis of Cu–Ag Composite Membrane Catalysts for Potassium Ferricyanide Reduction

This study investigates the catalytic properties of mono- and bimetallic composite track-etched membranes (CTeMs) fabricated using a galvanic replacement strategy. Two bimetallic architectures, Ag/Cu@PET and Cu/Ag@PET, were synthesized by sequentially depositing copper and silver onto poly(ethylene terephthalate) (PET) templates. X-ray diffraction analysis revealed that doping Cu@PET with silver nanoparticles formed a substitutional solid solution ($Ag_{97}Cu_3$), which increased crystallinity by >45 % compared to monometallic Cu@PET. In contrast, doping Ag@PET with copper produced a two-layer tubular structure with phase-separated copper co-deposited along silver microtubes. The catalytic performance was evaluated through the pseudo-first-order reduction of potassium ferricyanide (PFC) by sodium borohydride. The Cu/Ag@PET composite with separate phases demonstrated superior activity, achieving 94.3 % PFC reduction within 40 minutes, significantly exceeding the performance of monometallic Ag@PET and Cu@PET. Kinetic analysis indicated that the rate constant and activation energy strongly depended on membrane structure and silver doping time in case of formation of substitutional solid solution phase. A minimum doping duration of 20 minutes was required for performance enhancement, with 30-minute Ag/Cu@PET samples reducing activation energy from 62.35 kJ/mol to 32.67 kJ/mol. These findings highlight the critical role of metal deposition order and structural configuration in optimizing catalytic activity, demonstrating the efficacy of galvanic replacement for designing high-performance, multi-metallic membrane catalysts.

*Keywords:* composite, track-etched membranes, galvanic replacement, reduction, photocatalysts, bimetallic, poly(ethylene terephthalate), silver, copper

## *1. Introduction*

The development of hybrid and multicomponent nanostructured materials has gained increasing attention due to their superior performance compared to monometallic systems in fields such as catalysis, sensing, energy storage, and water purification [1–4]. Among various synthesis strategies, template-based electroless deposition provides a versatile and scalable approach to fabricate metal micro- and nanostructures with controllable dimensions and morphology [5, 6]. Depending on the type of redox pathway, the chemical deposition techniques within polymeric templates can be categorized into classical electroless deposition [7], galvanic replacement [8], and radiation-induced chemical reduction [9], as schematically summarized in Figure 1.

In electroless deposition, a reducing agent chemically reduces metal ions to form a metallic layer on the template surface. The process typically requires sensitization and activation steps and has been widely used for the fabrication of uniform metal microtubes inside track-etched membranes (TeMs). This technique allows for precise control over the geometry and composition of micro/nanotubes by adjusting factors such as temperature, time [10], and the composition of complexing agents in the plating bath [11, 12]. Notably, copper-based CTeMs have demonstrated significant promise in applications such as catalysis [13, 14], and heavy metal adsorption [15, 16].

Galvanic replacement (GR), is an efficient method of introducing a second, more noble metal into preformed structures of a less noble metal. During this spontaneous redox reaction, the less noble metal ($M_I$) serves as a sacrificial reductant, donating electrons to the more noble metal ion ($M_{II}$). This ion then deposits onto the surface while partially dissolving the base material [17, 18]. This process enables the synthesis of bimetallic and even trimetallic structures with improved catalytic, electronic, or optical properties. For ex-

© 2025 The Authors. This is an open access article under the CC BY-NC-ND license (http://creativecommons.org/licenses/by-nc-nd/4.0/)

ample, a $Cu_2O$/ZnO@PET composite was previously synthesized using this method, forming a multiphase material with a solid-solution phase of CuZn and enhanced photocatalytic performance [19].

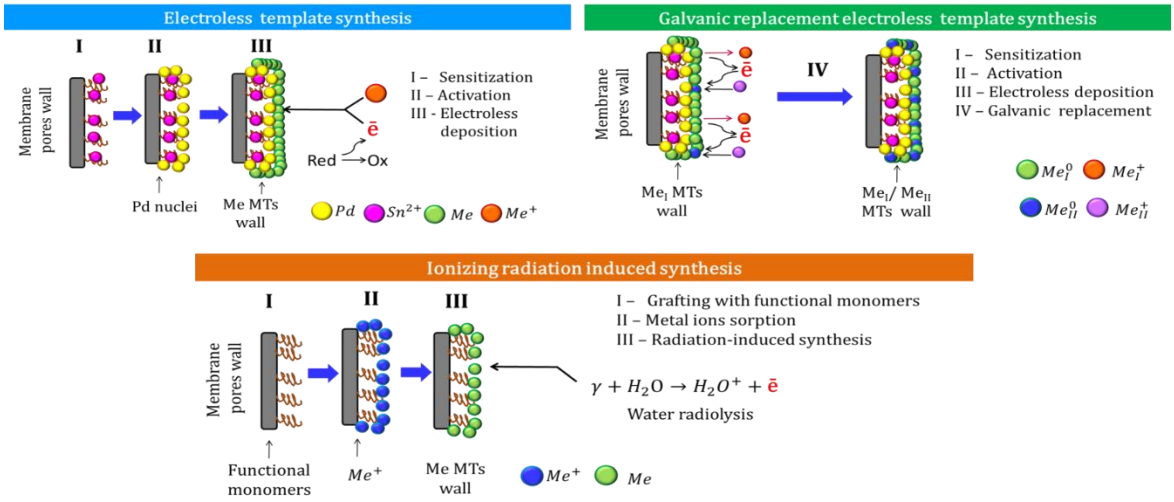


Figure 1. Schemes of CTeM synthesis using different synthesis approaches

Radiation-induced synthesis is an alternative approach that uses high-energy radiation (e.g., γ-rays, e-beam) to generate solvated electrons for the in-situ reduction of metal ions immobilized on functionalized templates. This technique has been successfully used to synthesize various metallic nanostructures including copper [20], silver, and gold [21] within grafted polymer matrices. However, its application is more specialized and often requires elaborate pretreatment steps.

While many of these methods have been explored individually, fewer studies have systematically examined the effect of combining sequential deposition and galvanic replacement strategies within the same membrane system. In particular, bimetallic systems such as Ag/Cu or Cu/Ag, where one metal overlays the other, offer potential synergistic effects due to modified surface electronic structures and enhanced interfacial reactivity. In this study, we explore for the first time the catalytic performance of Ag/Cu@PET and Cu/Ag@PET composite TeMs synthesized via a combination of electroless plating and galvanic replacement. The structural features, crystallinity, and phase composition of these materials are correlated with their ability to catalyze the reduction of potassium ferricyanide (PFC), a model inorganic pollutant.

PFC is a redox-active compound known for its environmental persistence and toxicity [22, 23]. In aqueous systems, PFC acts as a stable source of highly toxic Fe(III) [24], which upon reduction to Fe(II) becomes significantly less harmful and can even be beneficial to metabolic processes [25]. The Fe(III) to Fe(II) reduction is relevant not only for environmental detoxification but also in various industrial processes such as tin refining copper extraction [26], wine and citric acid production [27], pigment formation [28, 29], antioxidant activity [30], and chemical sensing [31].

Previously, we demonstrated that Cu-based CTeMs synthesized via electroless deposition with ascorbic acid could achieve over 90 % conversion of Fe(III) to Fe(II) in PFC solutions [32]. Building upon this work, we hypothesize that doping such structures with a second metal via galvanic replacement could lower activation barriers, increase electron transfer rates, and improve overall catalytic efficiency. We therefore investigate both Ag/Cu@PET and Cu/Ag@PET configurations to assess how synthesis pathway and metal combination influence catalytic activity, crystallinity, and morphology. To the best of our knowledge, this is one of the first comparative studies to systematically examine the effects of metal sequence (Cu → Ag vs. Ag → Cu), doping time, and solid solution formation ($Ag_{97}Cu_3$) in the context of PFC reduction using CTeMs. The results may offer valuable insights into the design of next-generation multicomponent membrane catalysts for environmental applications.

## *2. Experimental*

### *2.1 Chemicals*

All chemicals were used as received without further purification. Analytical grade reagents including copper(II) sulfate pentahydrate ($CuSO_4 \cdot 5H_2O$), silver nitrate ($AgNO_3$), formaldehyde ($CH_2O$), sodium boro-

hydride ($NaBH_4$), potassium ferricyanide ($K_3[Fe(CN)_6]$), sodium-potassium tartrate ($KNaC_4H_4O_6·4H_2O$), pyridine, and palladium chloride ($PdCl_2$) were purchased from Sigma-Aldrich. Deionized water (resistivity 18.2 MΩ·cm, Aqualon D–301) was used throughout all experiments.

*2.2 Synthesis of Composite Track-Etched Membranes (CTeMs)*

Commercial poly(ethylene terephthalate) (PET) track-etched membranes with a nominal thickness of 12 μm and a pore density of $4×10^7$ pores/cm$^2$ were used as the template. Following chemical etching in 2.2 M NaOH at 70 °C, gas permeability analysis determined the average pore diameter to be 410±12 nm. Prior to metal deposition, the membranes were sensitized and activated using standard procedures. For silver plating, the PET templates were immersed sequentially in sensitization solution (50 g/L $SnCl_2$ in 60 mL/L concentrated HCl for 15 min) and activation solution (59 mM $AgNO_3$ and 230 mM $NH_3$ for 3 min) [33]. For copper plating, a more robust activation protocol was applied, consisting of three sequential sensitization-activation cycles [34]. Composite membranes were fabricated in two configurations: (i) Ag/Cu@PET: Silver was deposited onto Cu@PET templates using a galvanic exchange reaction in an $AgNO_3$-containing bath; (ii) Cu/Ag@PET: Copper was deposited onto Ag@PET templates via galvanic replacement in a $CuSO_4$/formaldehyde bath. The detailed compositions of the plating baths, pH, temperature, and deposition times are summarized in Table 1.

Table 1

**Experimental details of the synthesis of composite TeMs**

| Composite | Plating Bath Composition | Plating Conditions | | | Ref. |
|---|---|---|---|---|---|
| | | Adjusted pH | *T* (°C) | Plating Time (min) | |
| Ag@PET | $AgNO_3$ (17 mM), potassium tartrate (120 mM), pyridine (50 mM) | – | 3 ± 1 | 300 | [33] |
| Cu@PET | $CuSO_4·5H_2O$ (5 g/L), $KNaC_4H_4O_6·4H_2O$ (18 g/L), NaOH (7 g/L), $CH_2O$ (0.13 M) | 12.45 ($H_2SO_4$) | 3 ± 1 | 40 | [34] |
| Cu/Ag@PET | Same as Cu plating bath, using Ag@PET as the template | 12.45 ($H_2SO_4$) | 3 ± 1 | 20 | This work |
| Ag/Cu@PET | Same as Ag plating bath, using Cu@PET as the template | – | 3 ± 1 | 5–30 | |

*2.3 Catalytic Activity Evaluation*

Catalytic activity was assessed by measuring the reduction of potassium ferricyanide (PFC) using sodium borohydride in aqueous medium. A 2×2 cm$^2$ CTeM sample was immersed in a 1:1 mixture of PFC ($6.0×10^{-5}$ M, 20 mL) and $NaBH_4$ ($5.3×10^{-3}$ M, 20 mL). The reaction was carried out at room temperature with gentle stirring. Aliquots (350 μL) were withdrawn at 10-minute intervals, and the optical absorbance at 420 nm was recorded using a Specord-250 spectrophotometer (Analytik Jena, Germany) in the wavelength range of 250–500 nm.

The reduction percentage (*D*, %) was calculated using:

$$D, \% = \frac{C_0 - C_t}{C_0} \times 100\ \% = \frac{A_0 - A_t}{A_0} \times 100\ \%, \quad (1)$$

where $A_0$ and $A_t$ are the absorbance values at time 0 and time *t*, respectively, and $C_0$ and $C_t$ are the concentration values of PFC at the initial time and time *t* [13].

A series of experiments were conducted within the temperature range of 20 to 30 °C to investigate the influence of temperature on the catalytic efficiency of PFC reduction. The reduction reaction was monitored spectrophotometrically for each experiment, and the rate constants (*k*, in min$^{-1}$) were determined based on the pseudo-first-order kinetic model.

The activation energy ($E_a$) was calculated by applying the Arrhenius equation [19]:

$$\ln k = \ln A - \left(E_a / RT\right), \quad (2)$$

where *k* is the apparent rate constant (min$^{-1}$), *A* is the pre-exponential factor, $E_a$ is the activation energy (J/mol), *R* is the universal gas constant (8.314 J/mol·K), and *T* is the absolute temperature in Kelvin (K). A linear plot of ln *k* versus 1000/*T* was constructed, and the slope ($-E_a/R$) was used to calculate the activation energy graphically.

*2.4 Investigation of the Composition and Structure of Composite Catalysts*

The morphology and dimensional features of the synthesized composite track-etched membranes (CTeMs) were examined using a JEOL JFC-7500F field-emission scanning electron microscope (FE-SEM). Prior to analysis, membrane samples were sputter-coated with a thin layer of gold to enhance conductivity. The energy-dispersive X-ray spectroscopy (EDX) was performed using a Hitachi TM3030 SEM equipped with a Bruker XFlash MIN SVE detector, operating at an acceleration voltage of 15 kV. Elemental mapping and point analysis were used to confirm the distribution and relative abundance of metal phases (Ag and Cu) within the composite membranes.

The inner diameters and wall thicknesses of the metal microtubes, as well as the initial pore size of the PET template, were estimated by gas-flow porometry. The calculation was performed using the Hagen–Poiseuille equation [35], which relates the pressure-driven gas permeability through cylindrical pores to their geometric dimensions. The deposition rate of copper ($R$) was calculated as the mass gain per unit area per hour, expressed in mg/cm$^2$·h, based on the difference in membrane weight before and after plating.

Crystallographic analysis of the deposited metallic structures was carried out using an X-ray diffractometer (Bruker D8 Advance, Germany) equipped with a Cu $K_\alpha$ radiation source ($\lambda$ = 1.5406 Å). XRD patterns were collected in the 2$\theta$ range of 30° to 80°, with a step size of 0.02° and a counting time of 1 second per step. The system operated at 40 kV and 40 mA.

The average crystallite size ($L$) was estimated using the Scherrer equation, applied to the full width at half maximum (FWHM) of the most prominent diffraction peaks. The FWHM values were determined through peak fitting using pseudo-Voigt functions, which enabled accurate quantification of crystallinity and phase identification.

## *3. Results and Discussion*

*3.1 Synthesis and Structural Analysis of Composite TeMs*

The changes in the structural parameters of the synthesized mono- and bimetallic composite track-etched membranes (CTeMs) are summarized in Table 2. The data demonstrate that the deposition rates ($R$) obtained during the second stage of synthesis (i.e., galvanic replacement) were comparable for both Ag/Cu@PET and Cu/Ag@PET composites, with values of 0.557 and 0.593 mg/cm$^2$·h, respectively, in addition to Ag@PET (0.255 mg/cm$^2$·h) and Cu@PET (0.251 mg/cm$^2$·h) composites. These values indicate that the kinetics of metal substitution or secondary deposition are relatively unaffected by whether silver is deposited on copper or vice versa under the given conditions.

Despite similar deposition rates, the wall thickness of the Ag-based hybrid microtubes was found to be significantly higher than that of the Cu-based analogs. Specifically, the silver layer in Ag@PET was 120.6 ± 4.2 nm thick, which is almost double the thickness of the copper layer in Cu@PET (64.2 ± 10.9 nm). This discrepancy is likely attributed to differences in the precursor concentration, ion reduction potential, and metal nucleation/growth behavior in the respective plating baths.

Interestingly, for the Ag/Cu@PET composite, a notable reduction in the net silver mass increment ($\Delta m$ = 5.2 mg) was observed compared to the monometallic Ag@PET ($\Delta m$ = 25.5 mg). This decrease suggests that partial dissolution of the underlying copper microtubes occurs during galvanic replacement, reducing the overall mass gain. Such dissolution is consistent with the spontaneous redox nature of the galvanic process, where the less noble metal (Cu) acts as the sacrificial anode, donating electrons to reduce $Ag^+$ ions. A similar trend was reported in other galvanic systems where structural hollowing or mass loss accompanies deposition of a more noble metal [17].

Table 2

**Structural Parameters of Mono- and Bicomponent CTeMs**

| Sample | Inner Diameter of MTs (nm) | MT Wall Thickness (nm) | | Deposition Rate $R$ (mg/cm²·h) | | $\Delta m$ (mg) | |
|---|---|---|---|---|---|---|---|
| | | $l$(Cu) | $l$(Ag) | $R_{Cu}$ | $R_{Ag}$ | Cu | Ag |
| Ag@PET | 153.9±8.36 | – | 120.6±4.2 | – | 0.255 | – | 25.5 |
| Cu/Ag@PET | 144.4±1.8 | 56.9±0.9 | – | 0.593 | – | 7.9 | – |
| Cu@PET | 276.0±21.8 | 64.2±10.9 | – | 0.251 | – | 11.7 | – |
| Ag/Cu@PET* | 91.9±5.0 | – | 31.3±2.5 | – | 0.557 | | 5.2 |
| *Deposition time for silver doping: 20 minutes. | | | | | | | |

Scanning electron microscopy (SEM) images (Fig. 3) confirmed the successful formation of hollow metal microtubes within the PET template in all samples. The observed tube structures were continuous and aligned along the template pores. There were distinguishable differences in wall thickness which were consistent with the porometry and gravimetric data presented in Table 2.

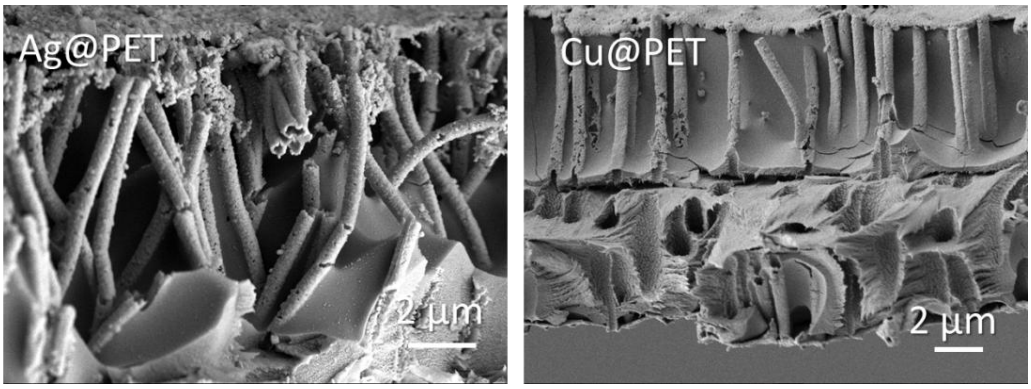


Figure 3. SEM images of cross sections of monocomponent CTeMs

The phase structure and crystallinity of the synthesized CTeMs were further analyzed using X-ray diffraction (XRD), and the results are presented in Table 3. The diffraction patterns for all samples (see Figure S1 in the Supplementary information file) showed good agreement with the standard JCPDS cards for face-centered cubic (fcc) silver (JCPDS 04-0783) and copper (JCPDS 04-0836), confirming the successful formation of the target phases.

Table 3

**Crystal Structure Parameters of CTeMs**

| Sample | Phase | Structure | Space group | *hkl* | 2θ (°) | *d* (Å) | *L* (nm) | FWHM | Lattice parameter (Å) | CD (%) | Phase content (%) | *V* (Å$^3$) |
|---|---|---|---|---|---|---|---|---|---|---|---|---|
| Ag@PET | Ag | Cubic | Fm-3m(225) | 111 | 38.20 | 2.35 | 36.33 | 0.26 | *a*=4.07408 | 76.5 | 100 | 67.62 |
| | | | | 200 | 44.25 | 2.05 | 24.45 | 0.39 | | | | |
| | | | | 220 | 64.48 | 1.44 | 35.13 | 0.30 | | | | |
| | | | | 311 | 77.36 | 1.23 | 33.98 | 0.33 | | | | |
| Cu/Ag@PET | Cu | Cubic | Fm-3m(225) | 111 | 43.49 | 2.08 | 28.04 | 0.34 | *a*=3.60662 | 79.6 | 27.9 | 46.91 |
| | Ag | Cubic | Fm-3m(225) | 111 | 38.05 | 2.36 | 33.20 | 0.28 | *a*=4.07889 | | 72.1 | 67.89 |
| | | | | 200 | 44.25 | 2.05 | 21.99 | 0.43 | | | | |
| | | | | 220 | 64.48 | 1.44 | 27.89 | 0.37 | | | | |
| | | | | 311 | 77.43 | 1.23 | 23.79 | 0.48 | | | | |
| | | | | 111 | 43.49 | 2.08 | 28.04 | 0.34 | | | | |
| | | | | 200 | 44.33 | 2.04 | 34.30 | 0.28 | | | | |
| | | | | 220 | 64.48 | 1.44 | 39.67 | 0.26 | | | | |
| | | | | 311 | 77.59 | 1.23 | 37.57 | 0.30 | | | | |
| | | | | 222 | 81.50 | 1.18 | 45.62 | 0.26 | | | | |
| Cu@PET | Cu | Cubic | Fm-3m(225) | 111 | 43.41 | 2.08 | 20.36 | 0.47 | *a*=3.60579 | 67.9 | 100 | 46.88 |
| | | | | 200 | 50.54 | 1.80 | 17.37 | 0.56 | | | | |
| | | | | 220 | 74.14 | 1.28 | 41.94 | 0.29 | | | | |
| Ag/Cu@PET | $Ag_{97}Cu_3$ | Cubic | Fm-3m(225) | 111 | 38.12 | 2.36 | 55.74 | 0.17 | *a*=4.08490 | 78.9 | 100 | 68.16 |
| | | | | 200 | 44.25 | 2.05 | 25.52 | 0.37 | | | | |
| | | | | 220 | 64.41 | 1.45 | 49.32 | 0.21 | | | | |
| | | | | 311 | 77.28 | 1.23 | 51.21 | 0.22 | | | | |
| | | | | 222 | 81.50 | 1.18 | 59.01 | 0.20 | | | | |

Changes in the full width at half maximum (FWHM) of the diffraction peaks provided insights into the degree of crystallinity (CD) and average crystallite size (*L*). The FWHM values were obtained by fitting the

peaks using symmetric pseudo-Voigt functions, allowing accurate deconvolution of overlapping reflections. As expected, broader peaks indicated smaller crystallite sizes and lower structural order, while narrower peaks suggested better-defined crystalline domains.

XRD analysis of the Ag/Cu@PET sample revealed the formation of a substitutional solid solution with the nominal composition $Ag_{97}Cu_3$ when Cu@PET was doped with silver nanoparticles. This membrane exhibited a high crystallinity degree (CD = 78.9 %) and large crystallite sizes (L), reaching to ≈ 59 nm, exceeding those observed in pure Cu@PET samples (CD = 67.9 %, L ≈ 20–42 nm). The lattice parameter of the $Ag_{97}Cu_3$ phase ($a$ = 4.0849 Å) was slightly expanded compared to pure Ag ($a$ = 4.0741 Å), reflecting Cu incorporation into the Ag lattice. In contrast, the Cu/Ag@PET membrane contained distinct and co-existing Cu and Ag phases without forming a solid solution. The copper phase exhibited smaller crystallites ($L$ ≈ 28 nm) and broader FWHM values, while the silver phase maintained relatively higher crystallinity. These observations are consistent with partial deposition of copper over a preformed Ag structure and are in line with previously reported galvanic systems [17].

These structural differences suggest that the route of deposition (Ag over Cu vs. Cu over Ag) significantly influences the resulting crystallinity and phase homogeneity of the composite membranes. The formation of a single-phase solid solution in Ag/Cu@PET, as opposed to phase-segregated structures in Cu/Ag@PET, is likely to impact their respective catalytic performances, which will be discussed in the subsequent sections.

The elemental composition and spatial distribution of metal phases within the CTeMs were examined via energy-dispersive X-ray spectroscopy (EDX) (Fig. 4). Elemental mapping revealed a uniform and continuous distribution of the deposited metals (Ag and Cu) throughout the microtube walls in all membrane types. Notably, even after the sequential doping of monometallic membranes, the second metal phase exhibited homogenous incorporation, without any evidence of phase segregation or surface agglomeration.

Point analysis from EDX indicated that the average atomic concentrations of the dopant elements were approximately 0.6 at.% for copper in Ag@PET, and 29.4 at.% for silver in Cu@PET, confirming the success of the galvanic replacement reactions and the effective incorporation of the secondary metal phase.

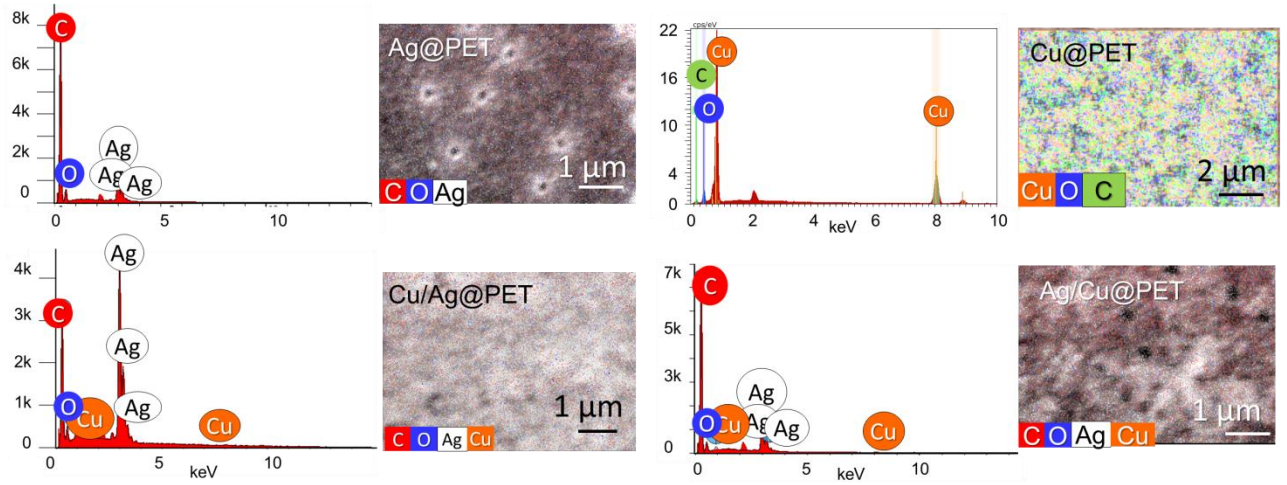


Figure 4. Energy-dispersive X-ray spectroscopy (EDX) analysis of CTeMs

*3.2 Evaluation of Catalytic Activity via PFC reduction*

The reduction of potassium ferricyanide ($K_3[Fe(CN)_6]$) was employed as a model reaction to assess the catalytic performance of the synthesized membranes. This system is widely used to evaluate redox-active nanomaterials due to its well-defined electrochemical behavior and straightforward spectrophotometric monitoring [36].

In this reaction, either sodium borohydride ($NaBH_4$) [25] or thiosulfate [37] acts as the reducing agent, converting ferricyanide ($Fe^{3+}$) to ferrocyanide ($Fe^{2+}$). This process is accompanied by a visible color change from yellow to colorless. The absorbance of Fe(III) species at 420 nm decreases progressively as the reaction proceeds, allowing real-time monitoring of the conversion degree. The overall redox reaction between ferricyanide and borohydride ions in aqueous solution is represented by the following equation [32].

$$BH_4^- + 8[Fe(CN_6)]^{3-} + 3H_2O \rightarrow H_3BO_3^- + 8[Fe(CN_6)]^{4-} + 8H^+ \quad (5)$$

This electron transfer is thermodynamically favorable due to the large difference in standard redox potentials: $E^0\left(Fe^{3+} \text{ in } [Fe(CN)_6]^{3-} / Fe^{2+} \text{ in } [Fe(CN)_6]^{4-}\right)$ is +0,44 V, while $E^0(BH_4^-/H_3BO_3)$ is –1,24 V. This results in a highly exergonic process ($\Delta G << 0$), which drives the reduction efficiently in the presence of an appropriate catalyst [32]. It is important to note that borohydride ions are also susceptible to hydrolysis, especially under acidic or neutral conditions, via:

$$BH_4^- + 2H_2O \rightarrow 4H_2 + BO_2^- \quad (6)$$

This side reaction competes with the desired redox process and may reduce the effective reducing capacity of the system. However, in the present study, the catalytic tests were conducted at pH ≈ 9, which significantly suppresses borohydride hydrolysis, rendering its effect negligible under experimental conditions.

Figure 5 shows the time-resolved UV–Vis absorption spectra for potassium ferricyanide (PFC) reduction, which were used to assess the catalytic efficiency of the synthesised CTeMs. The corresponding conversion efficiencies (*D*, %) are plotted in Figure 6. As expected, the monometallic Cu@PET membranes exhibited a high level of catalytic activity, achieving over 75 % reduction within the first 10 minutes of reaction. This observation is in agreement with previous studies that demonstrated the redox capabilities of copper microtubes prepared via electroless deposition [32]. When copper microtubes were subjected to galvanic replacement with silver to produce Ag/Cu@PET composites, XRD analysis confirmed that a substitutional solid solution ($Ag_{97}Cu_3$) had formed. As shown in Figure 6*a*, the catalytic activity of Ag/Cu@PET was initially lower than that of pure Cu@PET, especially during the early stages of the reaction. Although the final PFC conversion after 40 minutes was comparable (94.3 % for Ag/Cu@PET vs. 90.8 % for Cu@PET), the overall enhancement in performance was modest. This suggests that the formation of a structurally ordered $Ag_{97}Cu_3$ phase does not significantly enhance catalytic activity and may even inhibit it at shorter reaction times, possibly due to slower reduction rate as indicated by its lower rate constant ($k$) of $7.43\times10^{-2}$ $min^{-1}$, compared to $9.29\times10^{-2}$ $min^{-1}$ of Cu@PET (Section 3.3).

In contrast, the Cu/Ag@PET composites, composed of silver microtubes coated with a distinct ~60 nm copper layer, demonstrated a clear and substantial improvement in catalytic performance relative to their parent Ag@PET membranes. The monometallic Ag@PET system was the least active among all membranes tested, achieving only 79.4 % PFC reduction after 40 minutes. However, upon deposition of copper, the Cu/Ag@PET composites achieved up to 94.3 % conversion, reflecting a ~19 % improvement over Ag@PET. This performance gain can be attributed to the presence of physically separated Ag and Cu domains, rather than a uniform alloyed structure. The phase-separated nature of Cu/Ag@PET likely enables localized synergistic interactions at the Ag–Cu interfaces, facilitating enhanced electron transfer and increasing the density of catalytically active sites. Interestingly, while the $Ag_{97}Cu_3$ solid solution formed in Ag/Cu@PET is structurally well-defined, it does not outperform the heterogeneous phase structure of Cu/Ag@PET (27.9 % Cu and 72.1 % Ag). This indicates that structural order alone does not guarantee improved catalytic behavior; rather, interfacial effects and compositional heterogeneity may be more critical in determining activity.

Previous studies have shown that silver in close proximity to copper can stabilize copper in a partially oxidized $Cu^{\delta+}$ state, which binds reactants more strongly, thus enhancing surface reactivity [38, 39]. Additionally, silver nanoparticles are known to promote the reduction of surface copper oxides [40], leading to a process of in situ regeneration of active $Cu^0$ sites, which is a more efficient phase in catalyzing this type of reactions [14]. This mechanism is particularly effective in biphasic or phase-segregated systems such as Cu/Ag@PET, where mutual electronic interactions between adjacent Cu and Ag phases can continuously sustain catalytic performance.

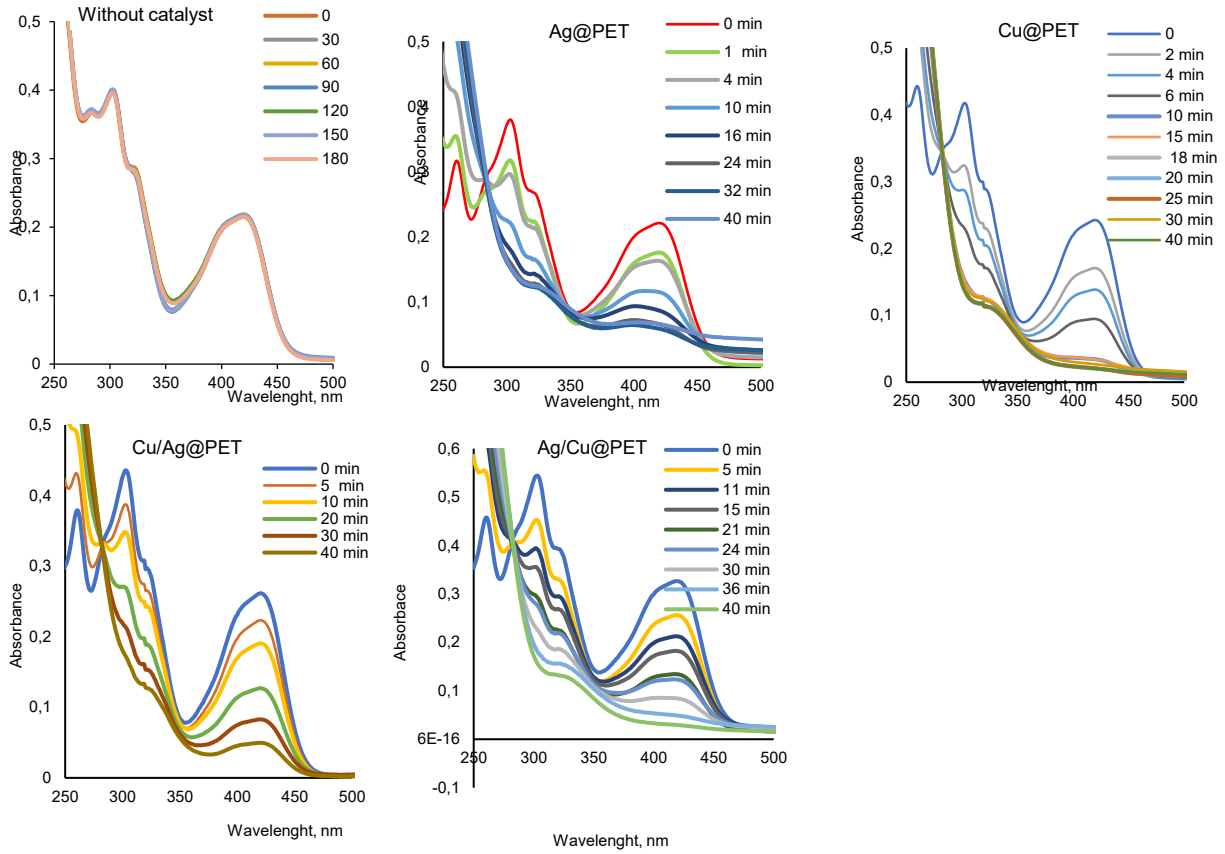


Figure 5. UV-Vis spectra of the PFC reduction reaction without the addition of a catalyst and in the presence of the studied composite catalysts

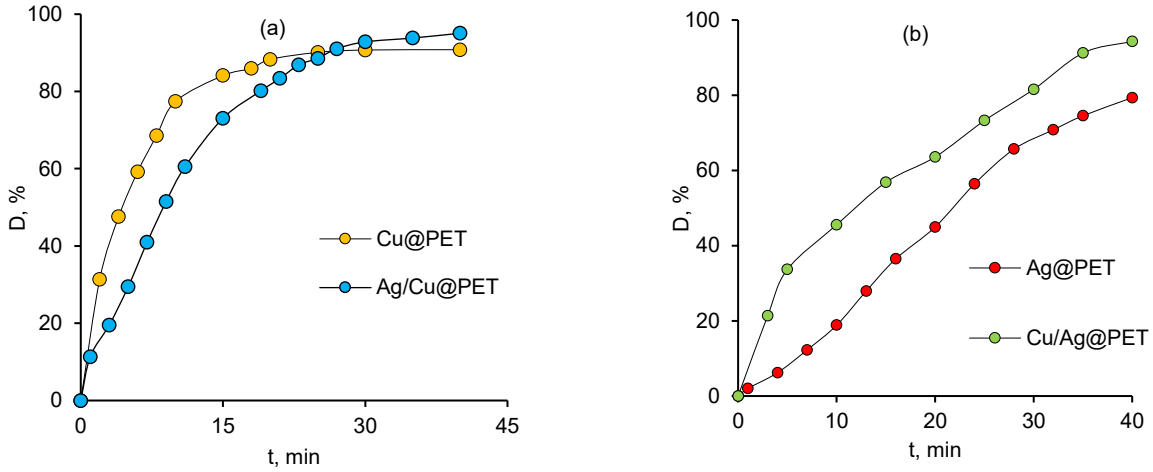


Figure 6. Change in the efficiency of PFC reduction for initial and modified samples based on MT of copper (*a*) and silver (*b*) (the doping time of the second component is 20 minutes)

*3.3 Kinetics, Doping Time Effect, and Activation Energy*

As expected for this class of redox reactions, the catalytic reduction of potassium ferricyanide (PFC) in the presence of nanoscale composite membranes was found to follow pseudo-first-order kinetics under conditions of excess sodium borohydride ($NaBH_4$), [32]. The rate constants ($k$) were determined from the slope of the linear plots of $\ln(C_0/C)$ versus reaction time ($t$), as shown in Figure 7. The high linearity of all curves confirms the proposed reaction order.

Among all studied membranes, the Ag@PET sample exhibited the lowest reaction rate constant, calculated as $3.48\times10^{-2}$ $min^{-1}$. In comparison, the Cu/Ag@PET composite, composed of a silver microtube sub-

strate coated with copper, exhibited a slightly higher rate of $3.92\times10^{-2}$ $min^{-1}$, indicating the beneficial influence of copper addition. Notably, the Cu@PET membranes demonstrated significantly greater reactivity, with a $k$ value of $9.29\times10^{-2}$ $min^{-1}$, consistent with the well-established redox behavior of copper surfaces. The Ag/Cu@PET membranes, featuring a solid solution structure of $Ag_{97}Cu_3$, a lower rate constant of $7.43\times10^{-2}$ $min^{-1}$ compared to its monometallic precursor membrane, i.e. Cu@PET.

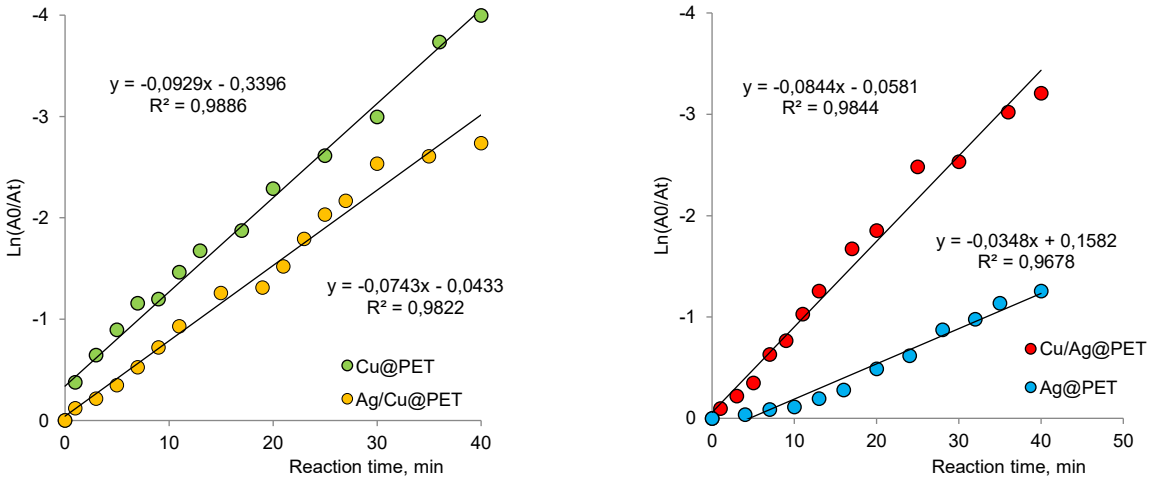


Figure 7. Kinetic curves of PFC reduction at 25 °C and change in the reaction rate constant for all types of composites studied

To investigate the effect of the time taken for silver doping on the catalytic performance of Ag/Cu@PET membranes, a series of samples were prepared with doping durations ranging from 5 to 30 minutes. The XRD analysis results in Table 4 confirmed that all samples had a cubic crystal structure corresponding to $Ag_{97}Cu_3$, with high degrees of crystallinity. However, a slight decrease in crystallinity (CD%) was observed as doping time increased. This reduction is likely due to the electroless deposition process, where thicker metal layers tend to become more amorphous within the confined pore geometry of the membrane.

Table 4

**Data on the structure and properties of Ag/Cu@PET composites with different doping times**

| Doping time, min | CD, % | MT wall width, nm | | Catalytic performance of CTeMs | | |
|---|---|---|---|---|---|---|
| | | $l$(Cu) | $l$(Ag) | $D$*, % | $k$, $min^{-1}$ | $E_a$, kJ/mol |
| 0 | 67.9 | 64.19±10.91 | 0 | 90.8 | 0.093 | 62.35 |
| 5 | 82.7 | | 26.11±6.13 | 67.7 | 0.032 | 69.24 |
| 10 | 81.4 | | 28.38±2.66 | 88.4 | 0.054 | 40.90 |
| 20 | 78.9 | | 31.30±2.50 | 94.3 | 0.074 | 35.00 |
| 30 | 74.5 | | 42.5±3.8 | 98.9 | 0.129 | 32.67 |
| * — at 25°C | | | | | | |

As presented in Figure 8, prolonged silver doping led to improved catalytic activity. Samples doped for 30 minutes achieved almost total PFC reduction (98.9 %) within 30 minutes, while those doped for less than 20 minutes showed only marginal gains compared to monometallic Cu@PET. Thus, a minimum doping threshold appears necessary to achieve significant enhancement in catalytic efficiency.

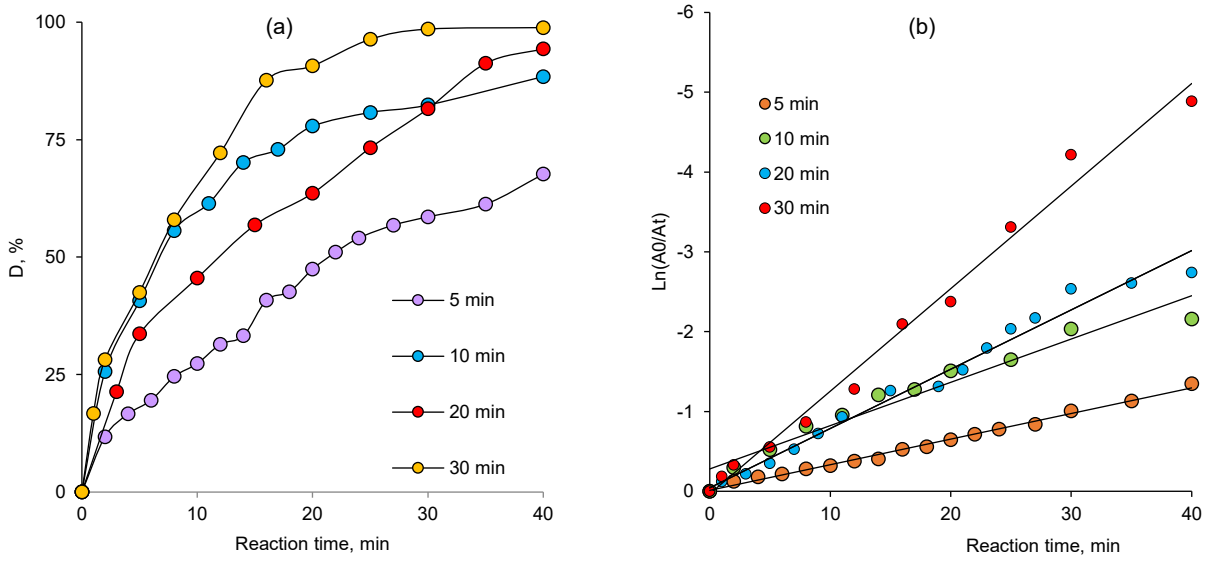


Figure 8. Change in the efficiency (*a*) and kinetic curves (*b*) of PFC reduction and change in the rate constant of the PFC reduction reaction in the presence of Ag/Cu@PET composites with different doping times

The activation energy ($E_a$) values, calculated from Arrhenius plots [41], further support this observation. A clear decreasing trend in $E_a$ was observed with increasing silver doping time (Table 4). The $E_a$ for the undoped Cu@PET sample was 62.35 kJ/mol, whereas the 30-minute doped Ag/Cu@PET membrane exhibited a markedly lower $E_a$ of 32.67 kJ/mol, corresponding to a reduction of over 47 %. This substantial decrease confirms that silver incorporation facilitates electron transfer, lowers energy barriers, and enhances reaction kinetics under the applied conditions. Although the reduction in Ea with increased silver doping time indicates improved electron transfer characteristics and more favorable reaction kinetics within the Ag/Cu@PET system, this does not necessarily translate to superior catalytic performance. Although the lower Ea indicates a reduced energy barrier for the redox reaction; however, catalytic activity is governed by a combination of kinetic and surface phenomena. In phase-separated structures such as Cu/Ag@PET, the presence of distinct Cu and Ag domains provide enhanced interfacial interactions, greater active surface area, and more efficient redox cycling between $Cu^0$ and $Cu^{\delta+}$ states. Thus, while Ag doping improves the intrinsic kinetics in Ag/Cu@PET, phase-separated architectures may remain more effective in promoting surface catalysis.

The issue of the stability of new catalysts is crucial when recommending them for further practical use outside the laboratory. Figure 9 shows the efficiency of PFC decomposition in the presence of the Cu/Ag@PET and Ag/Cu@PET (doping time — 30 min) composite membranes over multiple cycles. Notably, all samples maintained consistent performance across 5 test cycles without significant activity loss. After the 5th cycle, Cu/Ag@PET sample experienced around 8.7 % decline in degradation efficiency (*D* value). Similarly, the Ag/Cu@PET maintained exceptional stability, with only a 4.7 % reduction in efficiency over 5 cycles.

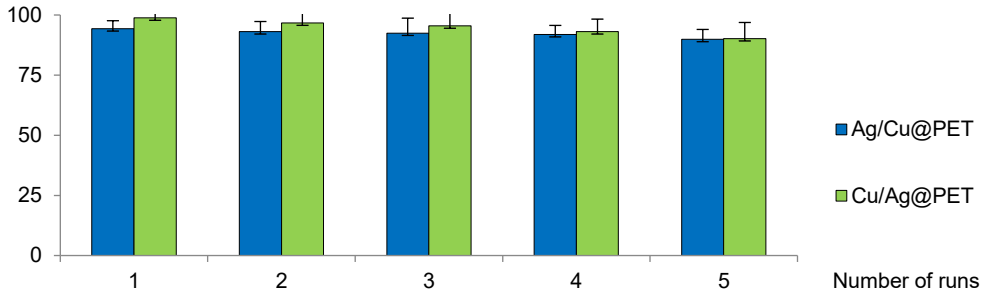


Figure 9. Catalyst reusability of composites membranes over multiple cycles (Experimental conditions: PFC concentration of $6.0\times10^{-5}$ M, temperature at 25 °C, reaction time — 40 min, catalyst membrane size of 2×2 cm)

## *Conclusions*

In this study, we demonstrated the use of the galvanic substitution method in the electroless synthesis of multicomponent composite track-etched membranes (CTeMs) as a template. It is shown that when MT copper is doped with silver nanoparticles, a solid substitution solution of the composition $Ag_{97}Cu_3$ with a high degree of crystallinity is formed. The formation of a two-layer MT of the composition Cu/Ag@PET is observed at the doping of the MT silver with copper nanoparticles. The effect of dopant phases on the catalytic properties of CTeM in the PFC reduction reaction showed that in both cases, polycomponent membranes accelerate the reaction under study more effectively than the initial samples.

Catalytic evaluation using potassium ferricyanide (PFC) reduction as a model reaction demonstrated that both bimetallic systems offered improved performance over monometallic Ag@PET. However, Cu/Ag@PET membranes outperformed all other configurations, achieving 94.3 % PFC reduction in 40 minutes. This enhancement is attributed to the synergistic effects at the Cu–Ag interface, where spatial phase separation promotes active site generation, electron transfer, and surface regeneration.

In contrast, Ag/Cu@PET membranes displayed only modest performance gains despite their high crystallinity. This suggests that single-phase alloy structures do not provide the same degree of catalytic synergy as heterogeneous phase interfaces. Kinetic studies confirmed pseudo-first-order behavior, and established a clear dependence of both the rate constant ($k$) and the activation energy ($E_a$) on membrane architecture and silver doping time was the time of silver doping. Importantly, Ag/Cu@PET samples doped for at least 20 minutes were necessary to observe significant performance gains. Membranes doped for 30 minutes showed nearly complete PFC conversion and an Ea reduction of over 47 % compared to undoped Cu@PET. These findings highlight the importance of both structural design and processing parameters in developing next-generation composite catalysts.

## *Supporting Information*

The Supporting Information is available free at https://ejc.buketov.edu.kz/index.php/ejc/article/view/374/277

## *Funding*

This research was funded by the Science Committee of the Ministry of Science and Higher Education of the Republic of Kazakhstan (Grant No. BR28713053).

## *Author Information**

**The authors' names are presented in the following order: First Name, Middle Name and Last Name*

**Saniya Renatovna Rakisheva** — Engineer, Technological Track-Etched Membranes Laboratory, Institute of Nuclear Physics of the Republic of Kazakhstan, Ibragimov Street, 1, 050032, Almaty, Kazakhstan; e-mail: saniya.rakisheva58@gmail.com; https://orcid.org/0000-0003-3618-4828

**Dinara Temirbayevna Nurpeisova** — PhD, Senior Lecturer, Chemistry Department, L.N. Gumilyov Eurasian National University, Satpayev street, 2, 010008 Astana, Kazakhstan; e-mail: nurpeisova_dt_1@enu.kz; https://orcid.org/0000-0001-8789-1798

**Alisher Madiyevich Zhumabayev** — Engineer, Technological Track-Etched Membranes Laboratory, Institute of Nuclear Physics of the Republic of Kazakhstan, Ibragimov street, 1, 050032, Almaty, Kazakhstan; e-mail: a.zhumabayev@inp.kz; https://orcid.org/0009-0007-4431-5468

**Nursanat Parmanbek** — PhD, Engineer, Technological Track-Etched Membranes Laboratory, Institute of Nuclear Physics of the Republic of Kazakhstan, Ibragimov street, 1, 050032, Almaty, Kazakhstan; e-mail: nursanat0509@mail.ru; https://orcid.org/0000-0002-9860-1087

**Murat Barsbay** — Professor, PhD, Department of Chemistry, Hacettepe University, 06800, Ankara, Turkey; e-mail: mbarsbay@hacettepe.edu.tr; https://orcid.org/0000-0003-0788-4446

**Anastassiya Alexandrovna Mashentseva** (*corresponding author*) — Prof., PhD, head of the technological track-etched membranes laboratory, Institute of Nuclear Physics of the Republic of Kazakhstan, Ibragimov street, 1, 050032 Almaty, Kazakhstan; e-mail: a.mashentseva@inp.kz; http://orcid.org/0000-0003-4393-5845

*Author Contributions*

The manuscript was written through contributions of all authors. All authors have given approval to the final version of the manuscript. CRediT: **Saniya Renatovna Rakisheva and Alisher Madiyevich Zhumabayev** conceptualization, data curation, investigation, methodology, validation, visualization, writing-review & editing; **Dinara Temirbayevna Nurpeisova, Nursanat Parmanbek** data curation, formal analysis; **Anastassiya Alexandrovna Mashentseva** conceptualization, formal analysis, funding acquisition, resources, supervision, validation, writing-original draft, writing-review & editing; **Murat Barsbay** supervision, validation, writing-review & editing

*Conflicts of Interest*

The authors declare no conflict of interest.

References

1 Wellmann, P. J. (2021). The search for new materials and the role of novel processing routes. *Discover Materials*, *1*(1), 14. https://doi.org/10.1007/s43939-021-00014-y

2 Magliaro, J., Altenhof, W., & Alpas, A. T. (2022). A review of advanced materials, structures and deformation modes for adaptive energy dissipation and structural crashworthiness. *Thin-Walled Structures*, *180*, 109808. https://doi.org/10.1016/j.tws.2022.109808

3 Kumari, S., Raturi, S., Kulshrestha, S., Chauhan, K., Dhingra, S., András, K., Singh, T. (2023). A comprehensive review on various techniques used for synthesizing nanoparticles. *Journal of Materials Research and Technology*, *27*, 1739–1763. https://doi.org/10.1016/j.jmrt.2023.09.291

4 Baig, N., Kammakakam, I., & Falath, W. (2021). Nanomaterials: a review of synthesis methods, properties, recent progress, and challenges. *Materials Advances*, *2*(6), 1821–1871. https://doi.org/10.1039/D0MA00807A

5 Lahiri, A., Pulletikurthi, G., & Endres, F. (2019). A Review on the Electroless Deposition of Functional Materials in Ionic Liquids for Batteries and Catalysis. *Frontiers in Chemistry*, *7*, 85. https://doi.org/10.3389/fchem.2019.00085

6 Muench, F. (2023). Direct surface functionalization with metal and metal oxide nanostructures. In *Encyclopedia of Nanomaterials* (pp. 318–336). Elsevier. https://doi.org/10.1016/B978-0-12-822425-0.00048-8

7 Felix, E., Muench, F., & Ensinger, W. (2014). Green plating of high aspect ratio gold nanotubes and their morphology-dependent performance in enzyme-free peroxide sensing. *RSC Adv.*, *4*(47), 24504. https://doi.org/10.1039/c4ra03377a

8 Schaefer, S., Muench, F., Mankel, E., Fuchs, A., Brötz, J., Kunz, U., & Ensinger, W. (2015). Double-Walled Ag — Pt Nanotubes Fabricated by Galvanic Replacement and Dealloying: Effect of Composition on the Methanol Oxidation Activity. *Nano*, *10*(06), 1550085. https://doi.org/10.1142/S179329201550085X

9 Parmanbek, N., Aimanova, N. A., Mashentseva, A. A., Barsbay, M., Abuova, F. U., Nurpeisova, D. T., … & Zdorovets, M. V. (2023). e-Beam and γ-rays Induced Synthesis and Catalytic Properties of Copper Nanoclusters-Deposited Composite Track-Etched Membranes. *Membranes*, *13*(7), 659. https://doi.org/10.3390/membranes13070659

10 Mashentseva, A. A., Kozlovskiy, A. L., Turapbay, K. O., Temir, A. M., Seytbaev, A. S., & Zdorovets, M. V. (2018). Determination of Optimal Conditions for Electoless Synthesis of Copper Nanotubes in the Polymer Matrix. *Russian Journal of General Chemistry*, *88*(6), 1213–1218. https://doi.org/10.1134/S1070363218060270

11 Muench, F., Rauber, M., Stegmann, C., Lauterbach, S., Kunz, U., Kleebe, H. -J., & Ensinger, W. (2011). Ligand-optimized electroless synthesis of silver nanotubes and their activity in the reduction of 4-nitrophenol. *Nanotechnology*, *22*(41), 415602. https://doi.org/10.1088/0957-4484/22/41/415602

12 Muench, F., Oezaslan, M., Svoboda, I., & Ensinger, W. (2015). Electroless plating of ultrathin palladium films: Self-initiated deposition and application in microreactor fabrication. *Materials Research Express*, *2*(10), 105010. https://doi.org/10.1088/2053-1591/2/10/105010

13 Mashentseva, A. A., Nurpeisova, D. T., & Barsbay, M. (2024). Effect of copper doping on the photocatalytic performance of $Ni_2O_3$@PC membrane composites in norfloxacin degradation. *RSC Advances*, *14*(7), 4424–4435. https://doi.org/10.1039/d3ra07471d

14 Nurpeisova, D. T., Mashentseva, A. A., Abuova, F., Aleskhanova, S. H., & Barsbay, M. (2025). Results in Materials Highly efficient CuO / Cu @ PC composite membranes for the photocatalytic degradation and sorption of roxithromycin from aqueous solutions. *Results in Materials*, *26*(June 2025), 100677. https://doi.org/10.1016/j.rinma.2025.100677

15 Altynbaeva, L. S., Mashentseva, A. A., Aimanova, N. A., Zheltov, D. A., Shlimas, D. I., Nurpeisova, D. T., … Zdorovets, M. V. (2023). Eco-Friendly Electroless Template Synthesis of Cu-Based Composite Track-Etched Membranes for Sorption Removal of Lead(II) Ions. *Membranes*, *13*(5), 495. https://doi.org/10.3390/membranes13050495

16 Russakova, A. V., Altynbaeva, L. S., Barsbay, M., Zheltov, D. A., Zdorovets, M. V., & Mashentseva, A. A. (2021). Kinetic and Isotherm Study of As(III) Removal from Aqueous Solution by PET Track-Etched Membranes Loaded with Copper Microtubes. *Membranes*, *11*(2), 116. https://doi.org/10.3390/membranes11020116

17 Cheng, H., Wang, C., Qin, D., & Xia, Y. (2023). Galvanic Replacement Synthesis of Metal Nanostructures: Bridging the Gap between Chemical and Electrochemical Approaches. *Accounts of Chemical Research*, *56*(7), 900–909. https://doi.org/10.1021/acs.accounts.3c00067

18 da Silva, A. G. M., Rodrigues, T. S., Haigh, S. J., & Camargo, P. H. C. (2017). Galvanic replacement reaction: recent developments for engineering metal nanostructures towards catalytic applications. *Chemical Communications*, *53*(53), 7135–7148. https://doi.org/10.1039/C7CC02352A

19 Altynbaeva, L., Barsbay, M., Aimanova, N., Jakupova, Z., Nurpeisova, D., Zdorovets, M., & Mashentseva, A. (2022). A Novel Cu2O/ZnO@PET Composite Membrane for the Photocatalytic Degradation of Carbendazim. *Nanomaterials*, *12*(10), 1724. https://doi.org/10.3390/nano12101724

20 Korolkov, I. V., Güven, O., Mashentseva, A. A., Atıcı, A. B., Gorin, Y. G., Zdorovets, M. V., & Taltenov, A. A. (2017). Radiation induced deposition of copper nanoparticles inside the nanochannels of poly(acrylic acid)-grafted poly(ethylene terephthalate) track-etched membranes. *Radiation Physics and Chemistry*, *130*, 480–487. https://doi.org/10.1016/j.radphyschem.2016.10.006

21 Korolkov, I. V., Mashentseva, A. A., Güven, O., Gorin, Y. G., Kozlovskiy, A. L., Zdorovets, M. V., … Cholach, S. O. (2018). Electron/gamma radiation-induced synthesis and catalytic activity of gold nanoparticles supported on track-etched poly(ethylene terephthalate) membranes. *Materials Chemistry and Physics*, *217*(April), 31–39. https://doi.org/10.1016/j.matchemphys.2018.06.039

22 Sut, M., Repmann, F., & Raab, T. (2014). Stability of Prussian Blue in Soils of a Former Manufactured Gas Plant Site. *Soil and Sediment Contamination: An International Journal*, *23*(5), 504–522. https://doi.org/10.1080/15320383.2014.839626

23 Pearce, J. (1994). Studies of any toxicological effects of Prussian blue compounds in mammals—A review. *Food and Chemical Toxicology*, *32*(6), 577–582. https://doi.org/10.1016/0278-6915(94)90116-3

24 Hantson, P., N'Geye, P., Laforge, M., Clemessy, J. -L., & Baud, F. (1996). Suicide Attempt by Ingestion of Potassium Ferricyanide. *Journal of Toxicology: Clinical Toxicology*, *34*(4), 471–473. https://doi.org/10.3109/15563659609013821

25 Veerakumar, P., Salamalai, K., Thanasekaran, P., & Lin, K. C. (2018). Simple Preparation of Porous Carbon-Supported Ruthenium: Propitious Catalytic Activity in the Reduction of Ferrocyanate(III) and a Cationic Dye. *ACS Omega*, *3*(10), 12609–12621. research-article. https://doi.org/10.1021/acsomega.8b01680

26 Paolella, A., Faure, C., Timoshevskii, V., Marras, S., Bertoni, G., Guerfi, A., … Zaghib, K. (2017). A review on hexacyanoferrate-based materials for energy storage and smart windows: challenges and perspectives. *Journal of Materials Chemistry A*, *5*(36), 18919–18932. https://doi.org/10.1039/C7TA05121B

27 Caballero, B., Toldra, P., & Fidel, F. (Eds.). (2003). *Encyclopedia of Food Sciences and Nutrition* (2nd-nd ed.). Academic Press Inc.

28 Huo, M., Zhao, R., Ying, Z., Jin, X., Zhu, Y., Wei, Q., & Ren, X. (2025). Efficient separation of $Fe^{3+}$ and $Cr^{3+}$ from chromium sludge leaching solution based on hydrogen bonding using trialkyl Phosphorus oxide. *Separation and Purification Technology*, *364*, 132462. https://doi.org/10.1016/j.seppur.2025.132462

29 Touzi, N., & Horchani-Naifer, K. (2023). A study on the preparation and characterization of pigment quality from mill scale steel wastes. *Environmental Science and Pollution Research*, *31*(28), 40538–40553. https://doi.org/10.1007/s11356-023-25594-5

30 Berker, K. I., Güçlü, K., Tor, İ., & Apak, R. (2007). Comparative evaluation of Fe(III) reducing power-based antioxidant capacity assays in the presence of phenanthroline, batho-phenanthroline, tripyridyltriazine (FRAP), and ferricyanide reagents. *Talanta*, *72*(3), 1157–1165. https://doi.org/10.1016/j.talanta.2007.01.019

31 Cheong, Y. H., Ge, L., Zhao, N., Teh, L. K., & Lisak, G. (2020). Ion selective electrodes utilizing a ferrocyanide doped redox active screen-printed solid contact — impact of electrode response to conditioning. *Journal of Electroanalytical Chemistry*, *870*, 114262. https://doi.org/10.1016/j.jelechem.2020.114262

32 Altynbaeva, L. S., Mendibaeva, A. Z., Aimanova, N. A., Nurmakhan, A. E., Dzhakupova, Z. E., Tuleuov, B. I., & Mashentseva, A. A. (2021). Kinetic and thermodynamic characteristics of the potassium hexationoferrate (III) decomposition catalytic reaction in the presence of composite track-etched membranes. *NNC RK Bulletin*, (1), 15–24. https://doi.org/10.52676/1729-7885-2021-1-15-24

33 Mashentseva, A. A., Barsbay, M., Aimanova, N. A., & Zdorovets, M. V. (2021). Application of Silver-Loaded Composite Track-Etched Membranes for Photocatalytic Decomposition of Methylene Blue under Visible Light. *Membranes*, *11*(1), 60. https://doi.org/10.3390/membranes11010060

34 Mashentseva, A. A. (2019). Effect of the Oxidative Modification and Activation of Templates Based on Poly(ethylene terephthalate) Track-Etched Membranes on the Electroless Deposition of Copper and the Catalytic Properties of Composite Membranes. *Petroleum Chemistry*, *59*(12), 1337–1344. https://doi.org/10.1134/S0965544119120089

35 Borgekov, D., Mashentseva, A., Kislitsin, S., Kozlovskiy, A., Russakova, A., & Zdorovets, M. (2015). Temperature Dependent Catalytic Activity of Ag/PET Ion-Track Membranes Composites. *Acta Physica Polonica A*, *128*(5), 871–875. https://doi.org/10.12693/APhysPolA.128.871

36 Susana, C. R., Jorge, P. J., Pablo, H., Luis, M. L. M., & Paul, M. (2010). Colloidal gold-catalyzed reduction of ferrocyanate (III) by borohydride ions: A model system for redox catalysis. *Langmuir*, *26*(2), 1271–1277. https://doi.org/10.1021/la902442p

37 Yen, C. W., & El-Sayed, M. A. (2009). Plasmonic field effect on the hexacyanoferrate (III)-thiosulfate electron transfer catalytic reaction on gold nanoparticles: Electromagnetic or thermal? *Journal of Physical Chemistry C*, *113*(45), 19585–19590. https://doi.org/10.1021/jp905186g

38 Martić, N., Reller, C., Macauley, C., Löffler, M., Reichert, A. M., Reichbauer, T., … Schmid, G. (2020). Ag2Cu2O3 — a catalyst template material for selective electroreduction of CO to C2+ products. *Energy & Environmental Science*, *13*(9), 2993–3006. https://doi.org/10.1039/D0EE01100B

39 Wang, L., Higgins, D. C., Ji, Y., Morales-Guio, C. G., Chan, K., Hahn, C., & Jaramillo, T. F. (2020). Selective reduction of CO to acetaldehyde with CuAg electrocatalysts. *Proceedings of the National Academy of Sciences*, *117*(23), 12572–12575. https://doi.org/10.1073/pnas.1821683117

40 Rollier, F. A., Muravev, V., Kosinov, N., Wissink, T., Anastasiadou, D., Ligt, B., … Hensen, E. J. M. (2025). Cu–Ag interactions in bimetallic Cu–Ag catalysts enhance C 2+ product formation during electrochemical CO reduction. *Journal of Materials Chemistry A*, *13*(3), 2285–2300. https://doi.org/10.1039/D4TA04263H

41 Kim, Y., Dumett Torres, D., & Jain, P. K. (2016). Activation Energies of Plasmonic Catalysts. *Nano Letters*, *16*(5), 3399–3407. https://doi.org/10.1021/acs.nanolett.6b01373